Resolving the time evolution of the dissociative nuclear wave packet in the repulsive state of H_2^+ via wave-packet interference

Pengkun Cao,[1] Qingbin Zhang,[1,*] Kunlong Liu [1,†] and Peixiang Lu[1,2]

[1]*School of Physics and Wuhan National Laboratory for Optoelectronics,*
Huazhong University of Science and Technology, Wuhan 430074, China

[2]*Hubei Key Laboratory of Optical Information and Pattern Recognition, Wuhan Institute of Technology, Wuhan 430205, China*

The temporal evolution of the dissociative nuclear wave packet (NWP) is intuitive for studying and understanding the dissociation mechanisms of molecules driven by laser fields. Yet, the time-domain information is encoded in the phase term of the wave function and is vanishing when the wave packet is being detected. Here, we demonstrate that the dynamic information for the dissociative NWP in the repulsive state of H_2^+ can be reconstructed using the wave-packet interference approach. In this approach, a reference pulse following the driving pulse is applied and creates a secondary dissociative NWP for coherent interference with the target NWP. By analyzing the modulation of the observed kinetic energy release distribution, we obtain the time-dependent yield of the target NWP and find a delay of its peak with respect to the field maximum. The delay is reduced when shorter or weaker driving pulses are applied. We attribute the delay to the competition between the three-photon and net-two-photon dissociation channels of H_2^+.

I. INTRODUCTION

Laser-induced molecular dissociation has attracted much attention in the past decades, as it provides a controllable way for studying and manipulating chemical reactions [1–3]. In particular, the understanding of the dynamics of small molecules driven by intense laser fields has advanced enormously [4]. The dissociation of H_2^+ has been mostly described within the two-state model, i.e., the attractive ground state $1s\sigma_g$ and the first repulsive $2p\sigma_u$ state. The typical dissociation pathways of H_2^+ in strong fields are sketched in Fig. 1. When exposed to a laser field, the nuclear wave packet (NWP) on the $1s\sigma_g$ potential curve starts vibrating. On one hand, when the NWP extends to the critical internuclear distance R_1 for three-photon coupling, the $2p\sigma_u$ state could be populated via three-photon absorption. The dissociative NWP on the repulsive state then moves towards a larger internuclear distance. In this case, the molecule would end up with dissociation in the $2p\sigma_u$ state directly (three-photon channel) or in the $1s\sigma_g$ state after emitting one photon at the internuclear distance R_2 of one-photon coupling (net-two-photon channel). On the other hand, when the vibrating NWP on the $1s\sigma_g$ potential curve further extends to R_2, the $2p\sigma_u$ state could be populated via one-photon absorption, eventually leading to the dissociation of the molecule in the $2p\sigma_u$ state (one-photon channel).

Generally, the dissociation channels of H_2^+ can be identified in the kinetic energy release (KER) spectra due to their distinguishable KER [5]. Yet, the KER spectra do not natu-

rally provide the information for resolving the time evolution of the dissociation reactions. In order to resolve the nuclear dynamics in molecular dissociation, Coulomb explosion imaging based on the pump-probe scheme was proposed [6,7]. By varying the time delay between the pump and probe pulses and measuring the delay-dependent KER of the Coulomb explosion fragments, the motion of the NWP was detected [7]. In this widely used approach, the delayed probe pulse is usually applied for measuring the dissociation process after the molecule interacts with the pump pulse [8,9]. This method demands that the pump pulse and probe pulse are well separated [8]. Therefore, it is not suitable for detecting the motion of the wave packet when the laser field is not finished. While resolving the time evolution of the ultrafast dynamics of dissociation has become more important and interesting [10], detecting when and how the dissociative NWP changes its pathway *within* the driving pulse is desired. This process occurs before the driving pulse is finished. Thus, it is difficult to detect by the traditional pump-probe scheme.

In this paper, we demonstrate that the dynamic information for the dissociative NWP in the repulsive state of H_2^+ during the interaction can be reconstructed by using wave-packet interference. The concept of wave-packet interference has been applied for detecting and controlling the electronic and nuclear dynamics driven by laser fields [11–16]. In our study, the dissociative NWP as the target one is generated by the driving pulse. Then, a reference pulse following the driving pulse is applied and creates a secondary dissociative NWP for coherent interference with the target one, eventually resulting in the interference pattern in the KER spectrum. Via analyzing the modulation of the KER distribution, the release time of the dissociative NWP for the three-photon dissociation channel is extracted. Based on the scheme of wave-packet interference,

*zhangqingbin@hust.edu.cn
†liukunlong@hust.edu.cn
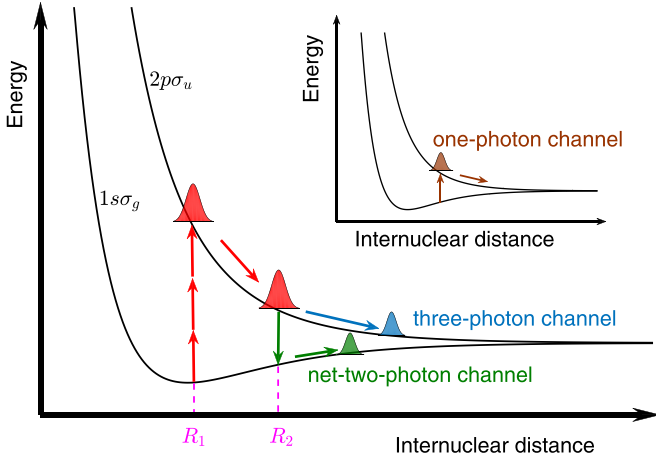
FIG. 1. Illustration of different dissociation channels of H_2^+ driven by laser fields. R_1 and R_2 indicate the internuclear distances where the three-photon coupling and the one-photon coupling occurs, respectively.

we find a delay of a few femtoseconds between the release of the dissociative NWP and the peak of the driving pulse envelope. We further show that such a delay is reduced when the driving pulse becomes weaker or shorter. Our analysis shows that the delay is associated with the competition between the three-photon and net-two-photon dissociation channels.

II. NUMERICAL METHOD

The photodissociation process of H_2^+ is mainly governed by the $1s\sigma_g$ and $2p\sigma_u$ electronic states, which are energetically well separated from other higher states. Therefore, as long as the applied laser field is not too high ($\leqslant 10^{14}$ W/cm^2), the calculation based on the two-level model for H_2^+ yields reasonable results [17]. Here, we solve numerically the two-dimensional, two-level, time-dependent Schrödinger equation (TDSE) [18] for H_2^+, which is written as (in the length gauge)

$$
i\frac{\partial}{\partial t}\begin{pmatrix}\psi_g(R_x, R_y, t)\\ \psi_u(R_x, R_y, t)\end{pmatrix}
$$

$$
= \begin{pmatrix}\frac{\hat{P}_x^2+\hat{P}_y^2}{2M}+V_g(R_x, R_y) & \mathbf{D}(R_x, R_y)\cdot\mathbf{E}(t)\\ \mathbf{D}(R_x, R_y)\cdot\mathbf{E}(t) & \frac{\hat{P}_x^2+\hat{P}_y^2}{2M}+V_u(R_x, R_y)\end{pmatrix}
$$

$$
\times\begin{pmatrix}\psi_g(R_x, R_y, t)\\ \psi_u(R_x, R_y, t)\end{pmatrix}, \tag{1}
$$

where $V_g(R_x, R_y)$ and $V_u(R_x, R_y)$ are the potential surfaces of the $1s\sigma_g$ and $2p\sigma_u$ states, respectively. $\mathbf{D}(R_x, R_y)$ is the transition dipole moment between two states. $\mathbf{E}(t)$ indicates the external electric field. In the present study, the dissociation is driven by the circularly polarized (CP) laser field, which is given by

$$
\mathbf{E}_1(t) = \mathcal{E}_1\sin^2\left(\frac{\pi t}{L_1}\right)[\cos(\omega_1 t)\hat{x} - \sin(\omega_1 t)\hat{y}], \tag{2}
$$

for $0 \leqslant t \leqslant L_1$, with ω, $\mathcal{E}$, and L_1 being the frequency, the electric field amplitude, and the full duration of the laser pulse. For the approach of wave-packet interference, the delayed

counter-rotating CP laser pulse as the reference one is given by

$$
\mathbf{E}_2(t) = \mathcal{E}_2\sin^2\left[\frac{\pi(t - t')}{L_2}\right]
$$

$$
\times\{\cos[\omega_2(t - t')]\hat{x} + \sin[\omega_2(t - t')]\hat{y}\}, \tag{3}
$$

for $0 \leqslant t - t' \leqslant L_2$. Note that t' should be no less than the full duration of the driving pulse so that the reference pulse is well separated from the driving one. In this paper, t' is set to be 35 fs, except for the calculation in Fig. 9. In Fig. 9, we discuss the effect of delay on the reconstruction results and the delays are set to be 35 and 20 fs, respectively. In the present demonstration, the same wavelength of 400 nm is adopted for both pulses, i.e., $\omega_2 = \omega_1$. In addition, the full duration of the reference pulse is fixed at four optical cycles. We vary the intensity and the duration of the driving pulse in our calculations, while we always keep $\mathcal{E}_2 = \mathcal{E}_1$.

In our simulations, the wave function is propagated in an 168 a.u. $\times$ 168 a.u. box with 2048 grids in each dimension. The time step is $\delta t = 0.2$ a.u. After the laser field is over, we keep propagating the wave function until the dissociative NWPs reach the region where $R > 20$ a.u., while the simulation box is large enough to avoid the reflection of the NWP at the boundary during the propagation. Finally, by filtering out the well-separated bound NWP, one can obtain the two-dimensional momentum distributions for the dissociative NWPs on the $1s\sigma_g$ and $2p\sigma_u$ potential surfaces, respectively, by applying the Fourier transformation. The angle-resolved KER distributions can be obtained as well from two-dimensional nuclear momentum distributions via a coordinate transformation.

III. SCHEME AND RESULTS

For the dissociation of H_2^+ driven by the circularly polarized laser pulse, the target dissociative NWP can be written as [17]

$$
\psi_{\text{target}} = A(K, \phi)e^{i[m\phi - K(t - t_0)]}, \tag{4}
$$

where $A(K, \phi)$ is the amplitude depending on the kinetic energy K and the angle ϕ. m is the angular momentum of the NWP; m will be increased (decreased) by one by absorbing one photon from the right (left) CP field. t_0 indicates the time when the target NWP is generated. The distribution of the KER is given by $|A(K, \phi)|^2$. Here, by measuring the KER spectra in a single driving pulse, one can obtain the information regarding the amplitude term of the wave function, but the information regarding the phase term is vanishing. In order to decode the information in the phase term, a short, counter-rotating CP pulse is applied at a delayed time to generate a reference NWP, which is written as

$$
\psi_{\text{ref}} = A'(K, \phi)e^{i[m'\phi - K(t - t'_0)]}. \tag{5}
$$

Then, the coherent superposition of the target and reference NWPs yields the KER distribution given by

$$
P(K, \phi) = |\psi_{\text{target}} + \psi_{\text{ref}}|^2
$$

$$
= |A|^2 + |A'|^2 + 2AA'\cos(\Delta m\phi - K\Delta t), \tag{6}
$$

with $\Delta m = m' - m$ and $\Delta t = t'_0 - t_0$. From Eq. (6), we can see that the phase information has been encoded in the in-
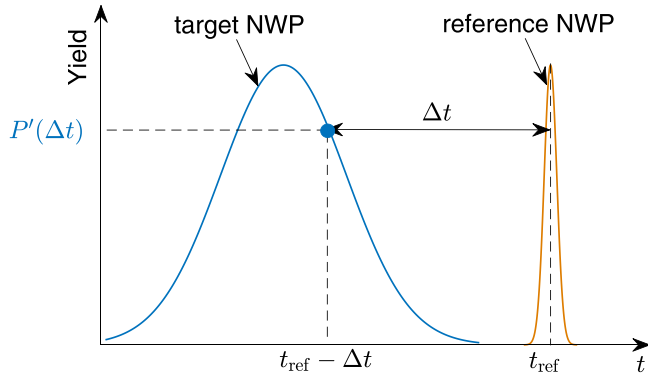
FIG. 2. The physical meaning of $P'(\Delta t)$ given by Eq. (8) is illustrated. t_{ref} is at the center of the reference NWP. $P'(\Delta t)$ is the reconstructed yield of the target NWP at the time $t_{\text{ref}} - \Delta t$.

terference term, which will lead to the modulation of the KER distribution. In a previous study, it was shown that one can extract Δm from the modulation of $P(\phi)$ and determine how many photons have been absorbed at a given kinetic energy [17]. In the present study, we will demonstrate that one can also extract the information regarding Δt from the KER distribution at a given angle. Here, we choose $\phi = 0$ and define

$$P_0(K) = \frac{P(K) - |A(K)|^2 - |A'(K)|^2}{2A'(K)} = A(K)\cos(-K\Delta t).$$

$$(7)$$

Then, by applying the Fourier transform to $P_0(K)$, we can obtain the distribution as a function of Δt as [14].

$$P'(\Delta t) = \left| \int P_0(K) \exp(iK\Delta t) dK \right|^2. \qquad (8)$$

The physical meaning of $P'(\Delta t)$ is illustrated in Fig. 2. If the reference pulse is short enough that the secondary dissociative wave packet (DWP) is distributed narrowly in time and approximately peaks at t_{ref} corresponding to the maximum of the reference pulse envelope, then $P'(\Delta t)$ in Eq. (8) can be understood as the relative yield of the target NWP generated at $t = t_{\text{ref}} - \Delta t$. In experiment, $P(K)$, $|A(K)|^2$, and $|A'(K)|^2$ can be measured by the commonly used detection apparatus [velocity map imaging (VMI) or cold-target recoil-ion-momentum spectroscopy (COLTRIMS)] [19–22]. Therefore, the time-dependent relative yield of the target NWP during the interaction can be reconstructed from the observables using the wave-packet interference approach.

To demonstrate our scheme, we solve numerically the TDSE given by Eq. (1) and obtain the KER distributions. The electric field of the right CP driving pulse [given by Eq. (3)] is depicted in Fig. 5(a). The corresponding angle-resolved KER distribution is shown in Fig. 5(b), where the right panel shows the KER distribution at $\phi = 0$. The KER spectrum within the given energy range (from 5.5 to 7.5 eV) peaks at around 6.7 eV, corresponding to the NWP dissociating through the three-photon channel. This NWP is our target wave packet and our goal is to decode when it is generated during the interaction. To this end, a short CP pulse [given by Eq. (3)] is applied following the driving pulse. The electric field for
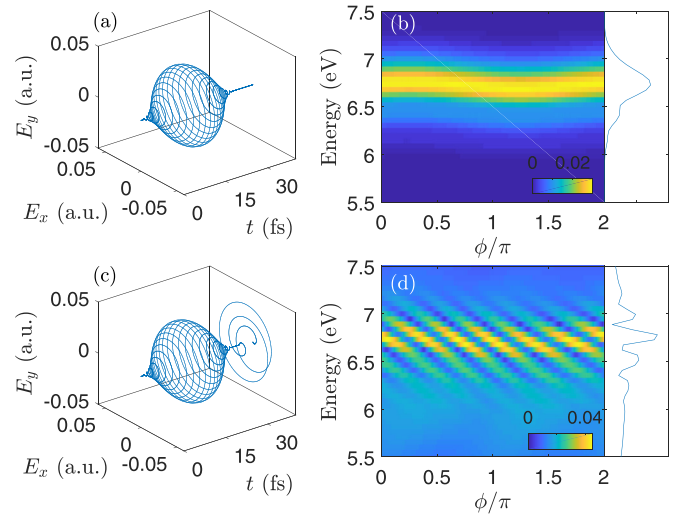
FIG. 3. (a) The electric field of the driving pulse. The wavelength, intensity, and pulse duration of the driving pulse are 400 nm, 10^{14} W/cm^2, and 33.36 fs, respectively. (b) The angle-resolved KER distribution corresponding to (a). The KER distribution at $\phi = 0$ is show in the right panel. (c) The electric fields of the driving pulse and the reference pulse. The wavelength, intensity, and duration of the reference pulse are 400 nm, 10^{14} W/cm^2, and 5.34 fs, respectively. (d) The angle-resolved KER distribution corresponding to (c). The KER distribution at $\phi = 0$ is shown in the right panel.

two sequential pulses is shown in Fig. 3(c) and the resulting KER distribution is shown in Fig. 3(d). We show on the right panel of Fig. 3(d) the KER distribution at $\phi = 0$ as well. In experiment, the driving laser pulse can be generated by the frequency doubling crystal and the reference laser pulse can be generated by the method in Ref. [23]. The H_2^+ on the ground vibrational state can be created by resonance-enhanced multiphoton ionization [24].

In Fig. 3(d), we can see from the KER distribution the tilted interference pattern, which is associated with the interference term of Eq. (6). By selecting the KER distribution at $\phi = 0$ and applying Eqs. (7) and (8), we obtain the relative yield of the target NWP as a function of Δt, i.e., $P'(\Delta t)$. The distribution, together with the pulse envelopes, is shown in Fig. 4, where t_{dri}, t_{ref}, and t_{tar} indicate the times when the driving pulse envelope, the reference pulse envelope, and the distribution $P'(\Delta t)$ reach their maxima, respectively. We find that there is a delay between t_{dri} and t_{tar}. For the given pulse parameters, the delay is about 4.5 fs. The result indicates that for the NWP eventually dissociating through the three-photon channel, its maximal yield is generated after the peak of the driving pulse.

We further apply the wave-packet interference scheme for the dissociation driven by the pulses of different parameters, focusing on the dissociative NWP of the three-photon channel. The time-dependent yields of the NWPs with respect to t_{dri} are shown in Fig. 5(a) for three pulse intensities and in Fig. 5(b) for three pulse durations, respectively. The vertical dashed line indicates the time corresponding to the maxima of the driving pulse envelopes. It is shown that the delay of the maximal yield with respect to t_{dri} is reduced for weaker pulse intensities and for shorter pulse durations.
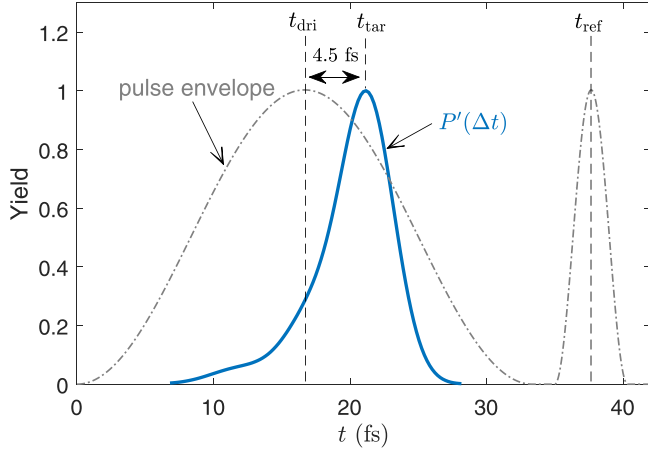
FIG. 4. The reconstructed yield distribution of the target NWP. The envelopes of the pulses are shown for comparison. t_{dri}, t_{ref}, and t_{tar} indicate the times when the driving pulse envelope, the reference pulse envelope, and the distribution reach their maxima, respectively. The laser parameters are the same as those in Fig. 3(c).

IV. DISCUSSION

The delayed generation of the NWP for the three-photon dissociation channel seems counterintuitive, as the maximum of the resonant population transfer from the ground state to the first excited state most likely takes place at the peak of the pulse intensity. In the following, before discussing the underlying mechanism leading to the delay, we verify the
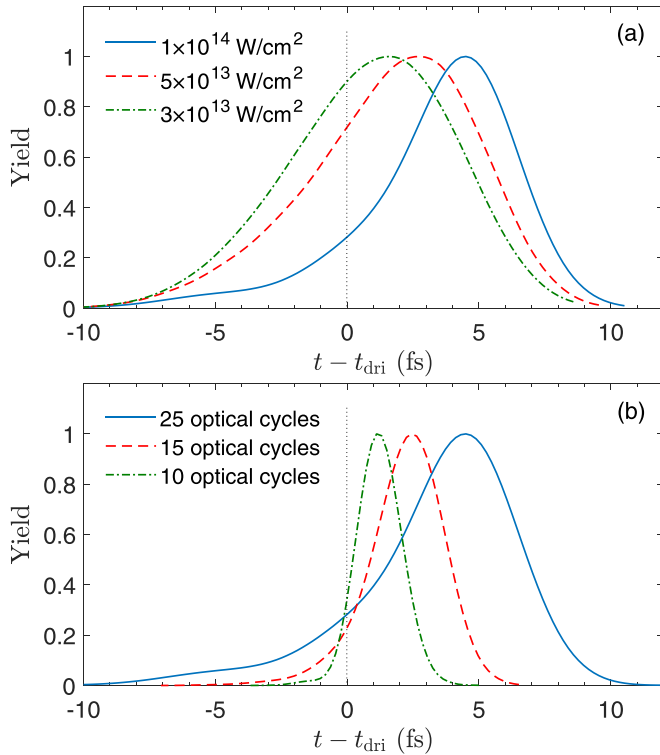
FIG. 5. The reconstructed yield distributions of the target NWPs as a function of $t - t_{\mathrm{dri}}$ for the driving pulses of different pulse intensities (a) and different pulse durations (b).
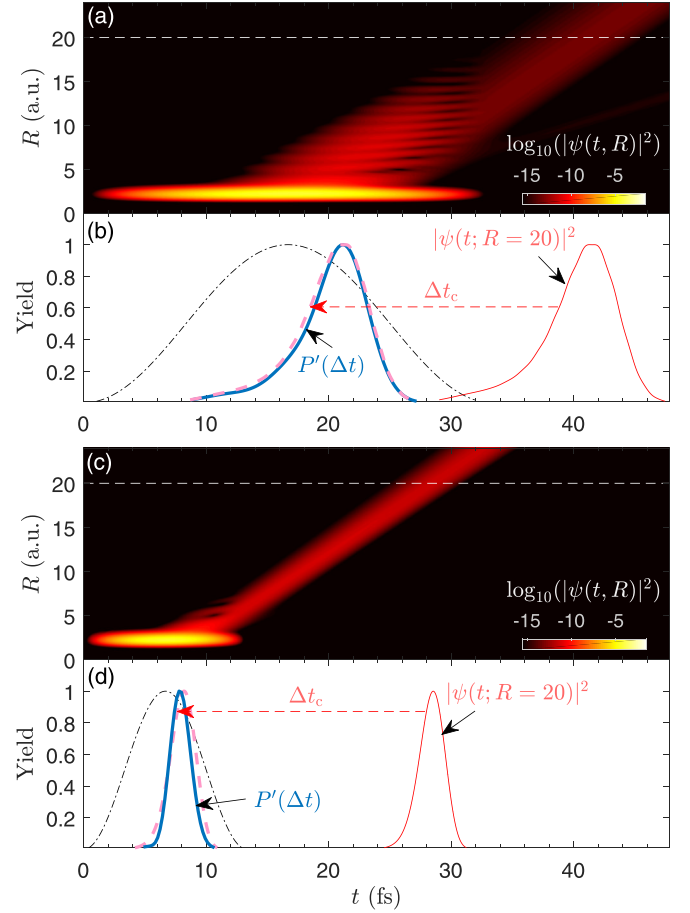
FIG. 6. The temporal evolution of the R-dimensional probability distributions in the $2p\sigma_u$ curve for pulses of (a) 25 optical cycles and (c) 10 optical cycles. The intensity and wavelength of laser pulse are 1×10^{14} W/cm^2 and 400 nm, respectively. The dashed line indicates $R = 20$ a.u. In (b) and (d), the envelope of driving pulse (dashed dotted curve), $P'(\Delta t)$ (thick solid curve), $|\psi_u(t; R = 20)|^2$ (solid curve), and $|\psi_u(t; R = 20)|^2$ shifted forward by Δt_c (dashed curve) corresponding to (a) and (c) are shown. Δt_c is the classical propagation time for the nuclei moving from $R = 2.3$ a.u. to $R = 20$ a.u.

wave-packet interference scheme by comparing $P'(\Delta t)$ obtained from the KER spectrum with the one extracted directly from the time-dependent wave function [25]. To this end, we calculate for the driving pulse alone the time evolution of the probability density $|\psi_u(t, R)|^2$, which is shown in Fig. 6(a). Then, we select the time-dependent distribution of the probability density at $R = 20$ a.u., as cut by the horizontal dashed line in the figure. The selected distribution $|\psi_u(t; R = 20)|^2$ is shown in Fig. 6(b) by the thin solid curve. Note that the kinetic energy of the dissociative NWP at $R = 20$ a.u. is already stable. By taking the mean kinetic energy known from the KER spectrum for the target NWP and the potential curve of the $2p\sigma_u$ state, we calculate classically the time Δt_c that the nuclei take to dissociate from the three-photon coupling point ($R = 2.3$ a.u.) to $R = 20$ a.u. The distribution $|\psi_u(t; R = 20)|^2$ shifted forward by Δt_c (approximately 20.2 fs from the classical calculation) is then depicted in Fig. 6(b) with the dashed curve. It is worth noting that the wave packet is not launched
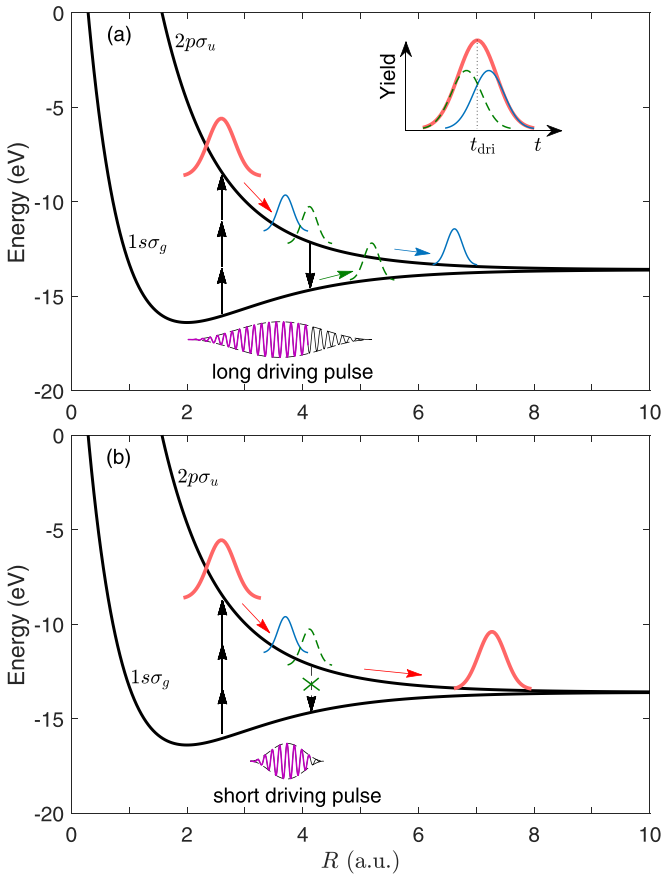
FIG. 7. The sketch of the dissociation process in (a) a long driving pulse and (b) a short driving pulse. Note that the shape of the DWP in this figure does not represent the real shape. See text for the details of the discussion.

FIG. 8. (a) The time-dependent normalized yield of DWP from the net-two-photon channel with different laser intensities. The yield of dissociative fragments from three-photon channel and net-two-photon channel in different laser durations (b) and intensities (c). The laser parameters are the same as those in Fig. 5. The yield has been normalized so that the total yield is 1.

at a certain "coupling point," but in a "coupling region." This leads to the fact that the propagation time of the wave packet to $R = 20$ a.u. is not a single value, but a distribution. Therefore, we use a single time (20.2 fs) to calculate the time when the wave packet is launched to the $2p\sigma_u$ state will introduce the error. We can estimate the value of this error by the KER distribution. From Fig. 3(b) we can obtain that the KER of the wave packet is mainly distributed in the range of 6.5–7 eV. This means that the initial internuclear distance distribution of the wave packet is about 2.26–2.34 a.u., and the propagation time ranges from 19.72 to 20.36 fs. We use a "shift time" of 20.2 fs for the whole wave packet, which results in an error of less than 0.5 fs. This error does not affect our main conclusions.

By comparing with $P'(\Delta t)$ (thick solid curve) reconstructed from the KER spectrum based on the wave-packet interference, we found fairly good agreement between the peak locations and the widths of two distributions. In addition, we repeat the procedure for the driving pulse of a different duration and the results are shown in Figs. 6(c) and 6(d) correspondingly. The reconstructed distribution and the calculated one are in good agreement as well, which further confirms the justification of the proposed wave-packet interference approach. Note that we have applied the assumption that the wave packet is launched to the $2p\sigma_u$ curve at $R = 2.32$

a.u. to calculate the propagation time. If the bandwidth of the laser pulse is quite broad, the NWP will be launched to the $2p\sigma_u$ state at a large range of internuclear distance, which will increase the computational errors. For a laser pulse of 10 optical cycles, the error of the propagation time is not more than 1.3 fs. This error is acceptable for our main conclusion.

Next, we discuss the reason for the delay between the peak of the reconstructed distribution and the peak of the driving pulse envelope. First, we assume that the population pumped to the $2p\sigma_u$ state at the internuclear distance corresponding to the three-photon coupling is a Gaussian distribution as a function of time and peaks at the electric field maximum, i.e., at t_{dri}, as shown by the thick curve in the inner figure in Fig. 7(a). Then, we further assume that the distribution is the sum of two sub-NWPs that peak before and after t_{dri}, respectively. As the dashed one is pumped earlier, it reaches the one-photon coupling point first when the external field of the long pulse is still strong enough to dump it to the ground state. In contrast, the sub-NWP indicated by the thin solid curve passes the one-photon coupling point at a delay time when the field is already weak, so it dissociates directly through the three-photon channel. In this case, the latter sub-NWP is the target being reconstructed, and thus there is a delay of the reconstructed NWP with respect to the field maximum. If the pulse is short enough or weak enough, as illustrated in Fig. 7(b), both sub-NWPs would pass the coupling point as the pulse would become weak by that time.
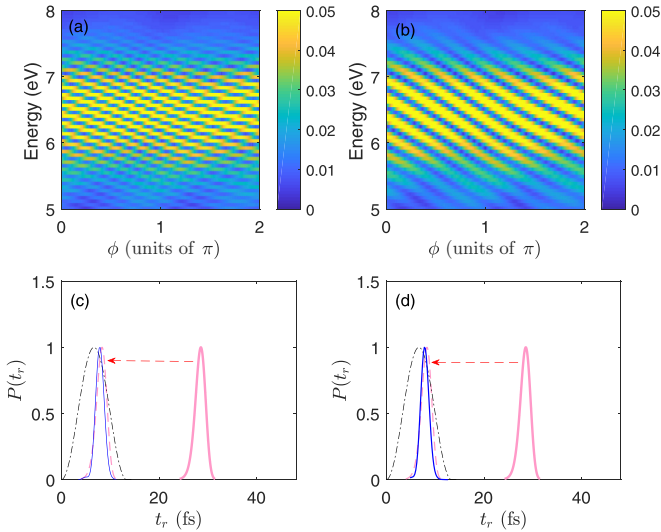
FIG. 9. Angle-resolved KER distributions with delay = 35 fs and delay = 20 fs are shown in (a) and (b), respectively. The reconstructed wave packet (blue solid curve) and the shift wave packet (red dashed curve) with delay = 35 fs and delay = 20 fs are shown in (c) and (d), respectively. The dotted black curve represents the envelope of the laser field.

Then, the full NWP would be the target and the delay of the reconstructed distribution should be close to zero. It explains the results shown in Figs. 5(a) and 5(b), where the peak of the reconstructed NWP distribution is closer to t_{dri} when the pulse intensity is lower or the pulse duration is shorter.

To verify our interpretation, we have calculated the time-dependent yield of NWP from the net-two-photon channel with different laser intensities and show it in Fig. 8(a). After the maximum of the driving laser, the NWPs on the $2p\sigma_u$ state begin to drop to the $1s\sigma_g$ state. In the stronger laser field, the process where the wave packet drops to the $1s\sigma_g$ state lasts for about 28 fs, but in the weaker laser field, the process lasts for about 24 fs. This leads to a relatively higher yield from the net-two-photon channel in the stronger laser fields. This is consistent with our explanation in Fig. 7. We also calculated the yields with different laser durations and intensities and show them in Figs. 8(b) and 8(c). In the weaker or shorter laser pulses, we can see that the yield from the net-two-photon channel decreases as the duration becomes shorter or the intensity decreases. This is due to the net-two-photon channel closing earlier in the shorter or the weaker laser pulse [see Fig. 7(b)]. The calculated result is consistent with our interpretation above.

In order to verify the applicability of our method to different delays, we perform the calculations with the same scheme but adopting the delay of 20 fs, as shown in Fig. 9. The angle-resolved KER distributions with delays of 35 and 20 fs are shown in Figs. 9(a) and 9(b), respectively. The interference

fringes are denser for a delay of 35 fs. This is due to the fact that the period of K is determined by Δt, as in Eq. (7). The reconstructed wave packets for delays of 35 and 20 fs are shown in Figs. 9(c) and 9(d). We can see that they are similar, which demonstrates that the wave packet can be reconstructed with different delays. It is necessary to note that the delay between the driving pulse and reference pulse should not be too short or too long. If the delay is too short, the reference pulse will overlap with the driving pulse. In this case, the pump pulse and probe pulse have been combined into a new laser pulse and interference cannot occur. If the delay is too long, the interference fringes are too dense to be resolve, because of the limitation of the detector's resolution.

In fact, the dissociation processes mentioned above have been discussed in the literature [26–30], and one can identify whether or not the above-threshold dissociation channels open simply from the KER spectra. Nevertheless, in the present study, we have shown that the dynamic information of the underlying process can be further revealed by applying the wave-packet interference approach. Since there is a time difference of a few femtoseconds between the dissociative fragments generated by the three-photon channel and the net-two-photon channel, we can further control the two channels by manipulating the pulse width and intensity of the laser pulse, or by tailoring the pulse shape. Our findings have potential applications in manipulating the reaction pathways.

V. CONCLUSION

In conclusion, we theoretically study the laser-induced dissociation dynamics of H_2^+ based on wave-packet interference. We demonstrate that the release time of the target NWP can be reconstructed by extracting the phase information from the interference fringes of the KER distribution. In the present study, we find that the NWP corresponding to the three-photon dissociation channel is released at a delay time with respect to the peak of the driving pulse. It is shown that the delay depends on the pulse duration and the intensity. We attribute it to the competition between the three-photon dissociation channel and the net-two-photon one. In experiment, our method can be implemented by probing the two-dimension momentum distribution of H_2^+. In addition, our approach does not require scanning the time delay between the driving pulse and the reference pulse, and thus it does not rely on high acquisition efficiency in experiment.

ACKNOWLEDGMENTS

[1] A. H. Zewail, J. Phys. Chem. A **104**, 5660 (2000).

[2] M. F. Kling, P. von den Hoff, I. Znakovskaya, and R. de Vivie-Riedle, Phys. Chem. Chem. Phys. **15**, 9448 (2013).

[3] R. N. Zare, Science **279**, 1875 (1998).

[4] J. H. Posthumus, Rep. Prog. Phys. **67**, 623 (2004).

[5] M. Kremer, B. Fischer, B. Feuerstein, V. L. B. de Jesus, V. Sharma, C. Hofrichter, A. Rudenko, U. Thumm, C. D. Schroter,

R. Moshammer, and J. Ullrich, Phys. Rev. Lett. **103**, 213003 (2009).

[6] H. Stapelfeldt, E. Constant, and P. B. Corkum, Phys. Rev. Lett. **74**, 3780 (1995).

[7] C. Trump, H. Rottke, and W. Sandner, Phys. Rev. A **59**, 2858 (1999).

[8] T. Ergler, A. Rudenko, B. Feuerstein, K. Zrost, C. D. Schröter, R. Moshammer, and J. Ullrich, Phys. Rev. Lett. **95**, 093001 (2005).

[9] T. Endo, S. P. Neville, V. Wanie, S. Beaulieu, C. Qu, J. Deschamps, P. Lassonde, B. E. Schmidt, H. Fujise, M. Fushitani, A. Hishikawa, P. L. Houston, J. M. Bowman, M. S. Schuurman, F. L. Légaré, and H. Ibrahim, Science **370**, 1072 (2020).

[10] C. R. Calvert, W. A. Bryan, W. R. Newell, and I. D. Williams, Phys. Rep. **491**, 1 (2010).

[11] N. F. Scherer, R. J. Carlson, A. Matro, M. Du, A. J. Ruggiero, V. Romero-Rochin, J. A. Cina, G. R. Fleming, and S. A. Rice, J. Chem. Phys. **95**, 1487 (1991).

[12] L. D. Noordam, D. I. Duncan, and T. F. Gallagher, Phys. Rev. A **45**, 4734 (1992).

[13] J. F. Christian, B. Broers, J. H. Hoogenraad, W. J. van der Zalde, and L. D. Noordam, Opt. Commun. **103**, 79 (1993).

[14] T. C. Weinacht, J. Ahn, and P. H. Bucksbaum, Phys. Rev. Lett. **80**, 5508 (1998).

[15] K. Ohmori, Annu. Rev. Phys. Chem. **60**, 487 (2009).

[16] D. DeMille, Phys. Rev. Lett. **88**, 067901 (2002).

[17] Z. Chen and F. He, Phys. Rev. A **102**, 033107 (2020).

[18] Z. Chen, P. L. He, and F. He, Phys. Rev. A **101**, 033406 (2020).

[19] A. Eppink and D. Parker, Rev. Sci. Instrum. **68**, 3477 (1997).

[20] D. Townsend, M. P. Minitti, and A. G. Suits, Rev. Sci. Instrum. **74**, 2530 (2003).

[21] S. K. Lee, F. Cudry, Y. F. Lin, S. Lingenfelter, A. H. Winney, L. Fan, and W. Li, Rev. Sci. Instrum. **85**, 123303 (2014).

[22] M. F. Kling, Ch. Siedschlag, A. J. Verhoef, J. I. Khan, M. Schultze, Th. Uphues, Y. Ni, M. Uiberacker, M. Drescher, F. Krausz, and M. J. J. Vrakking, Science **312**, 5771 (2006).

[23] F. Hu, Q. Zhang, J. Cao, Z. Hong, W. Cao, and P. Lu, Opt. Lett. **47**, 389 (2022).

[24] S. T. Pratt, Rep. Prog. Phys. **58**, 821 (1995).

[25] K. Liu, Q. Zhang, and P. Lu, Phys. Rev. A **86**, 033410 (2012).

[26] P. A. Orr, I. D. Williams, J. B. Greenwood, I. C. E. Turcu, W. A. Bryan, J. Pedregosa-Gutierrez, and C. W. Walter, Phys. Rev. Lett. **98**, 163001 (2007).

[27] J. McKenna, A. M. Sayler, F. Anis, B. Gaire, Nora G. Johnson, E. Parke, J. J. Hua, H. Mashiko, C. M. Nakamura, E. Moon, Z. Chang, K. D. Carnes, B. D. Esry, and I. Ben-Itzhak, Phys. Rev. Lett. **100**, 133001 (2008).

[28] A. Giusti-Suzor, X. He, O. Atabek, and F. H. Mies, Phys. Rev. Lett. **64**, 515 (1990).

[29] J. McKenna, F. Anis, A. M. Sayler, B. Gaire, N. G. Johnson, E. Parke, K. D. Carnes, B. D. Esry, and I. Ben-Itzhak, Phys. Rev. A **85**, 023405 (2012).

[30] H. Li, X. Gong, K. Lin, R. de Vivie-Riedle, X. M. Tong, J. Wu, and M. F. Kling, J. Phys. B **50**, 172001 (2017).